Neural dynamics of an extended frontal lobe network in goal-subgoal problem solving

Valentina Mione[1, 2] †

Jascha Achterberg[1] † ‡

Makoto Kusunoki[1, 2]

Mark J. Buckley[2]

John Duncan[1, 2] *

[1] MRC Cognition and Brain Sciences Unit, University of Cambridge, 15 Chaucer Road, Cambridge CB2 7EF, UK

[2] Department of Experimental Psychology, University of Oxford, Anna Watts Building, Radcliffe Observatory Quarter, Woodstock Road, Oxford, OX2 6GG, UK

† These authors contributed equally to the work.

‡ Present address: Centre for Neural Circuits and Behaviour, University of Oxford, 13 Mansfield Road, Oxford OX1 3SR, UK

* Correspondence: john.duncan@mrc-cbu.cam.ac.uk

Abstract

Complex behavior calls for hierarchical representation of current state, goal, and component moves. In the human brain, a network of "multiple-demand" (MD) regions underpins cognitive control. We recorded from four putative homologs to human MD regions in the frontal lobe – ventrolateral (vlPFC), dorsomedial (dmPFC), dorsal premotor (dPM) and insula/orbitofrontal (I/O) cortex - as monkeys solved an on-screen spatial maze. Across regions there was wide variation in strength of encoding task features. Sensory input and current state were strongly coded in vlPFC, goal most stably in dmPFC, and move most rapidly in vlPFC and dPM. I/O responded during revision of a prepared route. Across regions, an abstract, hierarchical code of problem structure marked progress from problem start to end. We suggest that, across an extended frontal network, partially separated but widely reproduced codes build the structured control program of organized behavior.

Introduction

Different anatomical connections give different regions of the primate frontal lobe partially specialized functions (*1*). At the same time, neurophysiological data often show overlapping response properties in different frontal regions (e.g. *2-4*), and dense connectivity within the frontal lobe suggests a medium for extensive information exchange (*5-6*). Across distributed frontal lobe networks, we still know little of specialised and overlapping functions as a complex cognitive control program unfolds.

Extended brain networks are well defined by human brain imaging. One robust discovery is a cortical/subcortical "multiple demand" (MD) network, recruited during many kinds of demanding cognitive activity, and linked to high-level cognitive control (*7-8*). Core components of this network are now tightly defined in several regions of lateral and dorsomedial frontal cortex, in the anterior insula, and within the intraparietal sulcus (*9*). Brain imaging data show frequent co-recruitment, strong functional connectivity, yet quantitative variations in activity pattern across the components of this network (*9*). Such findings suggest partial specialisation, but at the same time dense interaction and information sharing as cognitive operations are assembled and executed. In nonhuman primates, many studies document coding of diverse task features in lateral prefrontal, dorsomedial prefrontal, dorsal premotor and insular cortex (*4, 10-20*). Between regions, neural properties often overlap, though with quantitative differences (e.g. *4*, *10-13*, *17-18*). These findings, too, suggest that cognitive control rests on a distributed, interactive (*21*) network of multiple frontal lobe regions.

To extend these findings, we trained two macaques to solve problems in an on-screen maze, with each problem requiring a series of steps towards a rewarded goal. In this task, different routes

could lead to the same final goal, and different goals could be reached by partially overlapping routes. We recorded from four separate regions of frontal cortex, aiming for tentative homologs to human multiple-demand regions. Cognitive control rests on an internal model of a task's contents and requirements (*22-23*). This model must include a specification of current state, goal state, and actions chosen to reduce the difference between the two (*24-25*). Often behavior has a hierarchical structure, with a higher goal decomposed into a sequence of lower-level subgoals. All these aspects of the internal model must be integrated to direct behavioral choice. Across our extended frontal network, we examined the dynamics of specialised and overlapping neural coding for current state, goal, chosen moves and abstract problem structure. In contrast to studies focused on a specific aspect of frontal coding, we examined the full, complex structure of goal-directed behavior.

Results

The task is illustrated in fig. 1A. Problems were defined within a 5 x 5 maze, presented as a grid of lines on the computer screen. Maze locations were defined by intersections between these lines, comprising a central location, a surrounding inner square of 8 locations, and an outer square of a further 16 locations (fig. 1A, left). Monkeys began each problem fixating the center location, and were shown a goal placed at one of the 4 corners of the inner square. The task was to reach this goal with a series of saccades, each moving just one step through the maze. In fig. 1A, timings are shown to the right of the grid. The goal was shown for 900 ms, followed by a delay and then a pair of alternatives for the first step. Of the four inner ring locations adjacent to the start location, two (varying from problem to problem) were coloured green, indicating that they were available for selection, while the other two were coloured red, indicating unavailability. Following a further delay, the monkey made a saccade to the selected one of the

two green alternatives, the correct choice being the one moving closer to the goal. This process was then repeated for step 2 – delay, presentation of available and unavailable choices, further delay and saccade. For 2-step problems, one of the step 2 alternatives was the final goal, allowing the monkey to saccade to this goal for smoothie reward (fig. 1A, left). For 4-step problems, in contrast, the monkey was now forced to make a step to the outer ring. Two further choices, with similar timing, were required before the final goal was reached. The problem was always aborted for any error (see Materials and Methods), meaning that reducing numbers of trials were completed for each successive step.

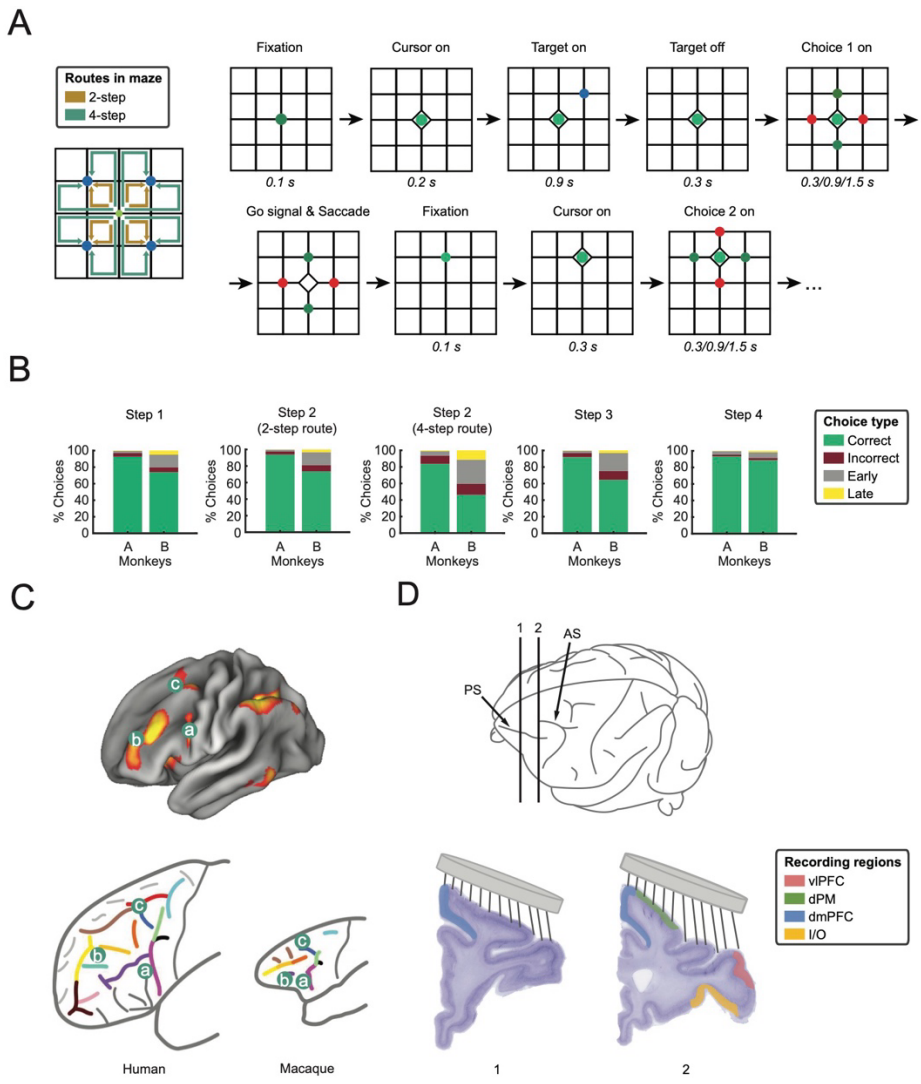

Fig. 1. Task, behavior and recording locations. A. Task. Left: The maze was presented as a grid of lines on a computer screen. The 5 x 5 maze locations were defined by intersections between these lines. At each step, the monkey made a saccade from current location (fixation point) to an immediately adjacent location. Green dot - starting location; blue dots – possible goal locations; arrows – 16 possible routes from start to goal (orange - 2-step; green - 4-step). Right: Timing of events from problem start to step 2 choice stimulus. Similar timings were used for each remaining step. B. Behavior. For each step, data are based on problems for which the corresponding choice stimulus was presented, i.e. excluding problems aborted at an earlier point. C. Correspondence analysis, suggesting putative match between human MD regions on lateral frontal surface and corresponding regions in macaque brain. Above – MD activity from (*9*), projected on partially inflated cortical surface. Green circles mark major MD regions. Below – putative sulcal correspondences between human and macaque, copied from (*26*). D. Recording regions illustrated on example coronal brain slices. PS – principal sulcus; AS – arcuate sulcus.

Behavioral results for the two animals are shown in fig. 1B. Except that monkey B often failed to wait for the go signal, the performance of both animals was accurate at each step. Discarding early and late responses, averaging across steps and problem types, the mean probability of correct choice was 0.95 for monkey A, 0.89 for monkey B.

Using a semi-chronic recording system, we recorded neural activity over 72 sessions in monkey A, 70 sessions in monkey B, with different groups of neurons recorded in each session. To target recordings we used current knowledge of human MD regions, combined with a recent analysis of correspondences between the frontal lobes of human, chimpanzee, baboon and macaque (*26*). On the lateral frontal surface, MD activity extends forward from the inferior frontal junction (fig. 1C, upper; circles ‘a’ and ‘b’) (*9*). The correspondence analysis (fig. 1C, lower) places the inferior frontal junction within the macaque ventrolateral prefrontal cortex (vlPFC), and based on a suggested correspondence between the macaque principal sulcus and the human posteromedial frontal sulcus, we tentatively match more anterior human MD regions also to macaque vlPFC. A further human MD patch is posterior and dorsal on the lateral frontal surface (fig. 1C, circle ‘c’), and the correspondence analysis suggests match to a region of dorsal premotor cortex (dPM),

behind the upper limb of the arcuate sulcus. On the dorsomedial surface, the human MD region overlaps presupplementary motor area (pre-SMA) and dorsal anterior cingulate; as a putative match we selected a region of dorsomedial prefrontal cortex (dmPFC) centered on the macaque pre-SMA. A highly consistent human MD region is found in the anterior insula and adjacent frontal operculum; as a tentative match, we recorded from a region of intermediate agranular insula and immediately adjacent orbitofrontal cortex (I/O). Based on the atlas of Saleem and Logothetis (*27*), our selected recording regions (fig. 1D) were thus vlPFC, including the anterior bank of the ventral arcuate sulcus (315 neurons, 236/79 from monkeys A/B, regions 45, 44, 8A-F5), dPM (341 neurons, 318/23 from monkeys A/B, regions F2, F7), dmPFC (360 neurons, 311/49 from monkeys A/B, regions F3, F6, 9m/8Bm), and I/O (358 neurons, 327/31 from monkeys A/B, regions Iai, 12o, 13l).

Sensory input

For a first comparison of regions, we examined responses to sensory input. In our maze problems, unpredictable input occurred at three points: at initial presentation of the goal, at step 1 when available alternatives indicated a horizontal or vertical first move, and at step 2 when alternatives indicated a 2- or 4-step route. In each case, for each individual neuron, we used analysis of variance (ANOVA) on spike rate to measure proportion of explained variance (PEV) for goal location during goal presentation, for horizontal/vertical choice available at step 1, and for 2- vs 4-step at step 2 (see Materials and Methods). ANOVAs were conducted on data from successive 50 msec windows, beginning 200 ms before each stimulus event. Randomisation tests (see Materials and Methods) were used to identify significant periods of information coding (PEV > 0) in each region, and to compare PEV between regions. Here and subsequently, analyses for each step included only data from trials on which this step was completed correctly.

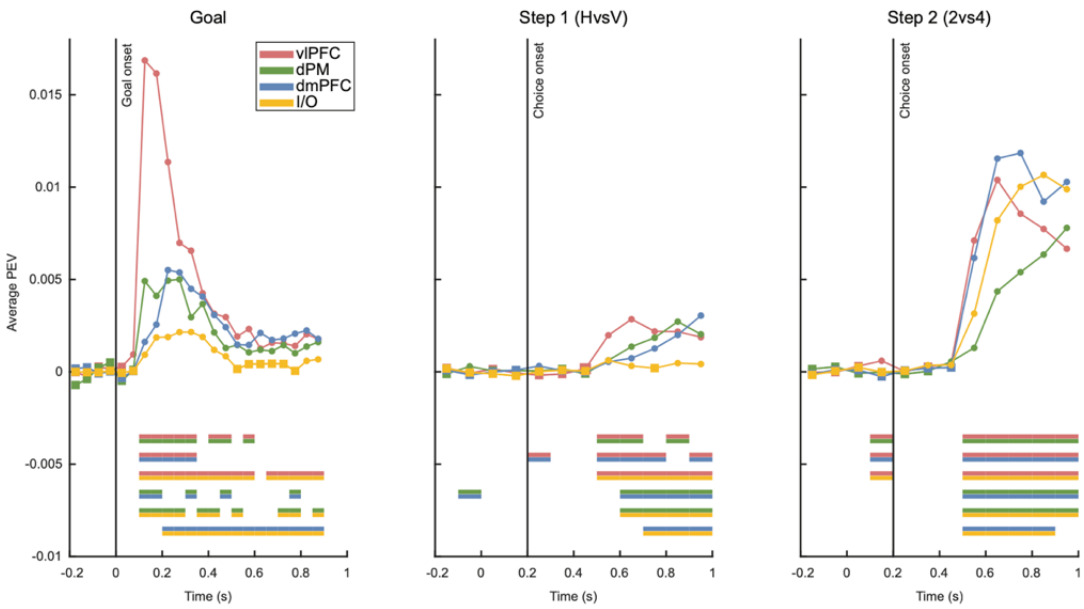

<u>Fig. 2</u>. Explained variance following sensory input. Mean proportion of explained variance (PEV) for goal (left, aligned at goal onset), horizontal (H) versus vertical (V) first move (middle, aligned at onset of choice 1 stimulus), and 2- versus 4-step problem (right, aligned at onset of choice 2 stimulus). For each region, values of PEV significantly > 0 ($p < .05$, FDR corrected) are indicated by round dots, nonsignificant by square dots. Horizontal bars (bottom) show significant differences between each pair of regions.

Mean values of PEV across all recorded neurons in each region are shown in fig. 2. For goal (fig. 2, left), an early peak in vlPFC, first significant in the window 50-100 ms post onset and maximal in the period 100-200 ms, was followed by rapid decline to a plateau lasting to the end of the goal presentation. In other regions, the peak developed more slowly, and most weakly in I/O, but again, goal coding remained largely significant to the end of the presentation period. For horizontal/vertical first move (fig. 2, middle), vlPFC again showed the strongest early coding, now beginning in the window 150-200 ms post onset of the choice alternatives, but by 250-300 ms, there was substantial convergence between vlPFC, dPM and dmPFC. For 2- vs 4-step coding at step 2 (fig. 2, right), coding onset was again fastest in vlPFC (150-200 ms window), but thereafter, coding became strongest in dmPFC and, slightly later, in I/O. In line

with human fMRI data, showing coactivation of MD regions, these results show substantial overlap in response of the four regions. At the same time they show clear functional separations, with vlPFC showing strong and rapid responses to all novel sensory input, and I/O strongly responsive only to an input differentiating immediate goal access from a longer, more demanding path.

Location spaces

For the next analyses we wished to define separate representational spaces for two aspects of the maze problem. For the first, we used combined data from steps 2 (2-step problems only) and 4, since combining these two steps, each possible goal (top left, top right, bottom left, bottom right) is associated with each possible move/saccade (left, right, up, down). For each goal, over a window extending from -200 to +100 ms from choice stimulus presentation, we averaged firing rates for each neuron over the four possible moves. For each region, we then used principal components analysis (PCA) to extract a representational space differentiating the four goal locations. Note that different goal locations were partially associated with different current locations (at steps 2 and 4, current location always immediately adjacent to final goal). We used data from steps 1 to 4 to disambiguate signals of goal and current location.

In each space, reflecting the two-dimensional layout of the maze, the first two PCs accounted for the great majority of variance (89, 91, 90, 84% respectively for vlPFC, dPM, dmPFC and I/O). For each region, for the combined data from steps 2 and 4, projections onto the first two PCs showed the expected structure, with the four locations organized in a layout approximately matching their spatial layout on the screen (fig. 3, top panel for each region).

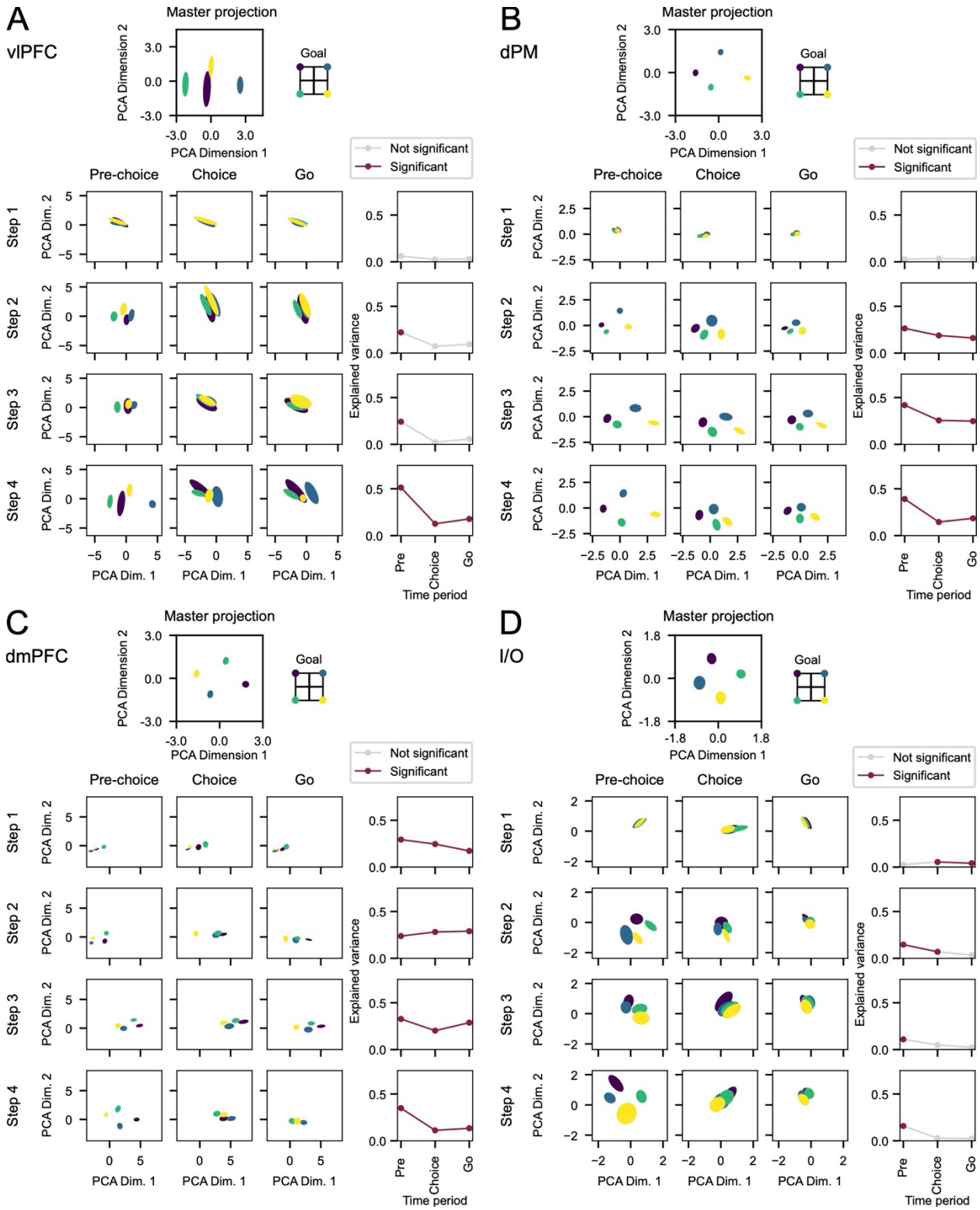

Fig. 3. **Location spaces**. A - vlPFC, B - dPM, C – dmPFC, D – I/O. For each region, the top panel shows projections into a master space derived from data averaged over four moves for each goal location (pre-choice periods from steps 2 (2-step problems only) and 4). Lower rows show projections into this master space for data from individual time windows in each step (left three panels), with proportion of explained variance in each window to the right (purple, $p < .05$,

FDR corrected). Step 2 row takes data only from 2-step problems. Ellipses show confidence intervals derived by bootstrap resampling.

With this space defined, we proceeded to examine projections from other problem periods. For each of the four steps separately, we took data from three periods: -200 to +100 ms from choice stimulus presentation (pre-choice), as used in the original creation of the spaces; +200 to +400 ms from choice stimulus (choice), to capture the movement selection period; and -200 to +100 ms from the go signal (go). For each region, the resulting projections for each goal are shown in the lower four rows of fig. 3, with the step 2 row using only data from 2-step trials (for similar results in 4-step trials, see fig. S1). In each row, the rightmost plot shows cross-validated proportion of variance explained by projections into the PCA space (see Materials and Methods).

For vlPFC (fig. 3, top left), there was a striking and unique pattern. At step 1, when the monkey always fixated the center location, projections of the four goal locations were not significantly different. Significant differences appeared from steps 2 to 4, especially in the pre-choice period of each step, but were by far the strongest at step 4. Notably, at step 4, current locations were maximally different for the four goals (outer ring locations adjacent to each goal).

For dmPFC (fig. 3, bottom left) there was a complementary pattern. For this region, the four goals were significantly and consistently separated from the period preceding step 1 to the pre-go period of step 4. A corresponding analysis of data from the early target presentation period (100 to 400 ms post onset of the goal stimulus at trial start) showed strong separation even here (proportion of explained variance 0.30), much greater than for other regions (0.05 to 0.08). For dmPFC, these results suggest a consistent representational space separating the four goals, established immediately at target presentation and maintained to problem end.

For dPM and I/O, results were a mixture of these two patterns. Again, projections of the four goals were closely similar at step 1, but then separated across later steps, again most strongly in the pre-choice period.

To further differentiate representations of goal and current location, we used data from the pre-choice period of steps 2 (2-step problems) and 3 (4-step problems). For these data, each goal was associated with one of two current locations, and each current location was associated with one of two goals. Projections of the resulting eight cases are shown in fig. 4, separately classified by current location and goal. Beneath these projections are shown mean distances between points with same goal/different current location, same current location/different goal, and as a comparison, both different (baseline). (Note that, for the first two cases, required moves were always different; for comparability, we also selected baseline pairs with different moves.) For vlPFC, distances were shortest for same current location/different goal, supporting the conclusion that, in this region, the coding space was predominantly concerned with current location. For dmPFC there was a complementary result, with shortest distance for same goal/different current location. For the remaining two regions, results suggested representation of both current location and goal.

Results for vlPFC are intriguing because, though goal location was strongly represented during initial target presentation (fig. 2), this did not translate into a later, stable goal space. This conclusion was confirmed by constructing a new goal space from the target presentation period (+100 to +400 ms from goal onset), and examining how much between-goal variance this space could explain in pre-choice periods from each subsequent step. Proportion explained variance was always below 0.13, and nonsignificant except for the period preceding step 2. To a large

extent, in vlPFC, the strong goal representation created during target presentation was lost in subsequent steps towards this goal.

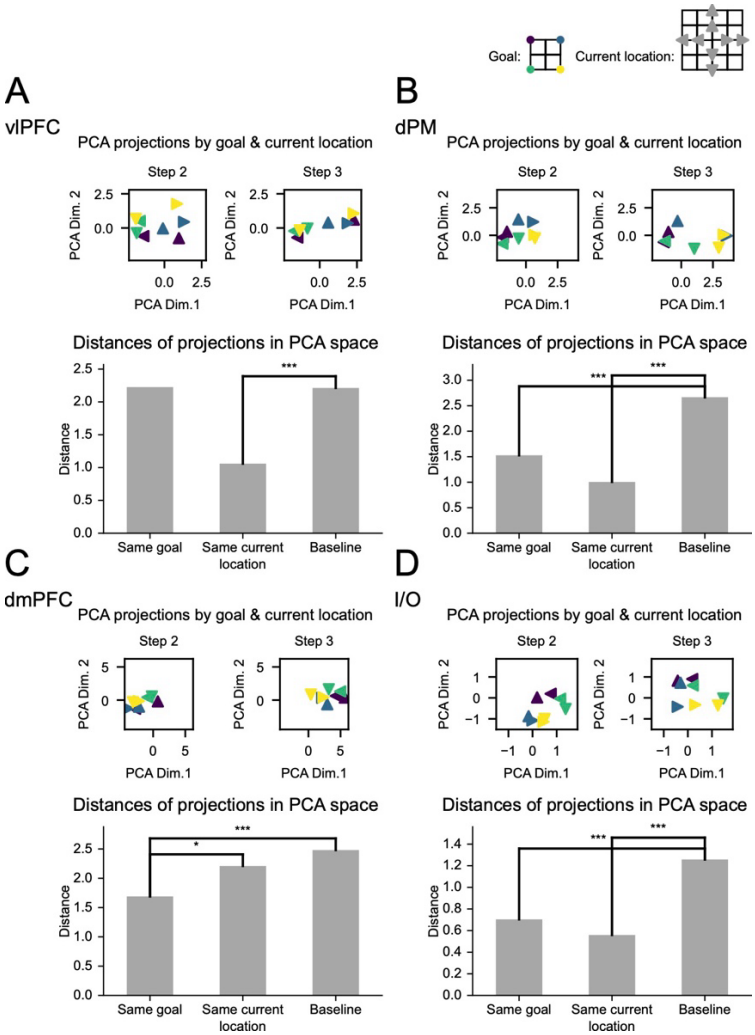

Fig. 4. Projections into master location space for pre-choice data from steps 2 (2-step problems) and 3. A - vlPFC, B - dPM, C – dmPFC, D – I/O. For each region, top panels show projections for data sorted by goal location x current location. Bottom shows mean distance between projections for pairs of points with same goal (different current location and move), same current location (different goal and move), and baseline (different goal, current location and move). * $p < .05$; *** $p < .001$.

Together, these results show a mixture of shared and specialised location coding. Strong coding of current location in the vlPFC may again reflect the influence of immediate visual input.

dmPFC was unique in carrying a stable goal code from problem start to end. In dPM and I/O, there was evidence for codes of both current and goal locations.

Move spaces

To define a move space we took a complementary approach. Again we combined data from steps 2 (2-step problems only) and 4, so that for each move, we could average data across the four different goals. To appropriately capture move selection we used the post-choice period, +200 to +400 ms from choice stimulus onset. For each region, once again, the great majority of variance was captured by the first two principal components (86, 88, 91, 76% respectively for vlPFC, dPM, dmPFC and I/O), and projections for the four possible moves approximated their objective spatial relations (fig. 5, top part of each panel). Confidence intervals (fig. 5, ellipses; see Materials and Methods) showed that move directions were discriminated much more weakly in I/O than other regions.

Fig. 5 (lower rows in each panel) shows projections for each problem step, sorting data for each step according to the move made on this step. For step 2, again, we show data just for 2-step trials (for 4-step problems, see below). Apart from weaker move coding in I/O, the results show broadly similar dynamics across regions. At step 1, as expected, projections for the four moves separated rapidly after onset of the choice stimulus (fig. 5, compare pre-choice with choice). In dmPFC, small but significant variations within the move space, even prior to onset of the choice stimulus, suggest preparatory bias towards the two possible moves associated with the current goal. At later steps, move coding was robust even prior to choice stimulus onset, indicating preparation of the forthcoming move. For step 2, the results show anticipatory selection of the move required in a 2-step problem, i.e. the move that would reach the final goal. For steps 3 and

4, the required move was 100% predictable. At each step, move coding strengthened after onset of the choice stimulus, and remained up to the go period.

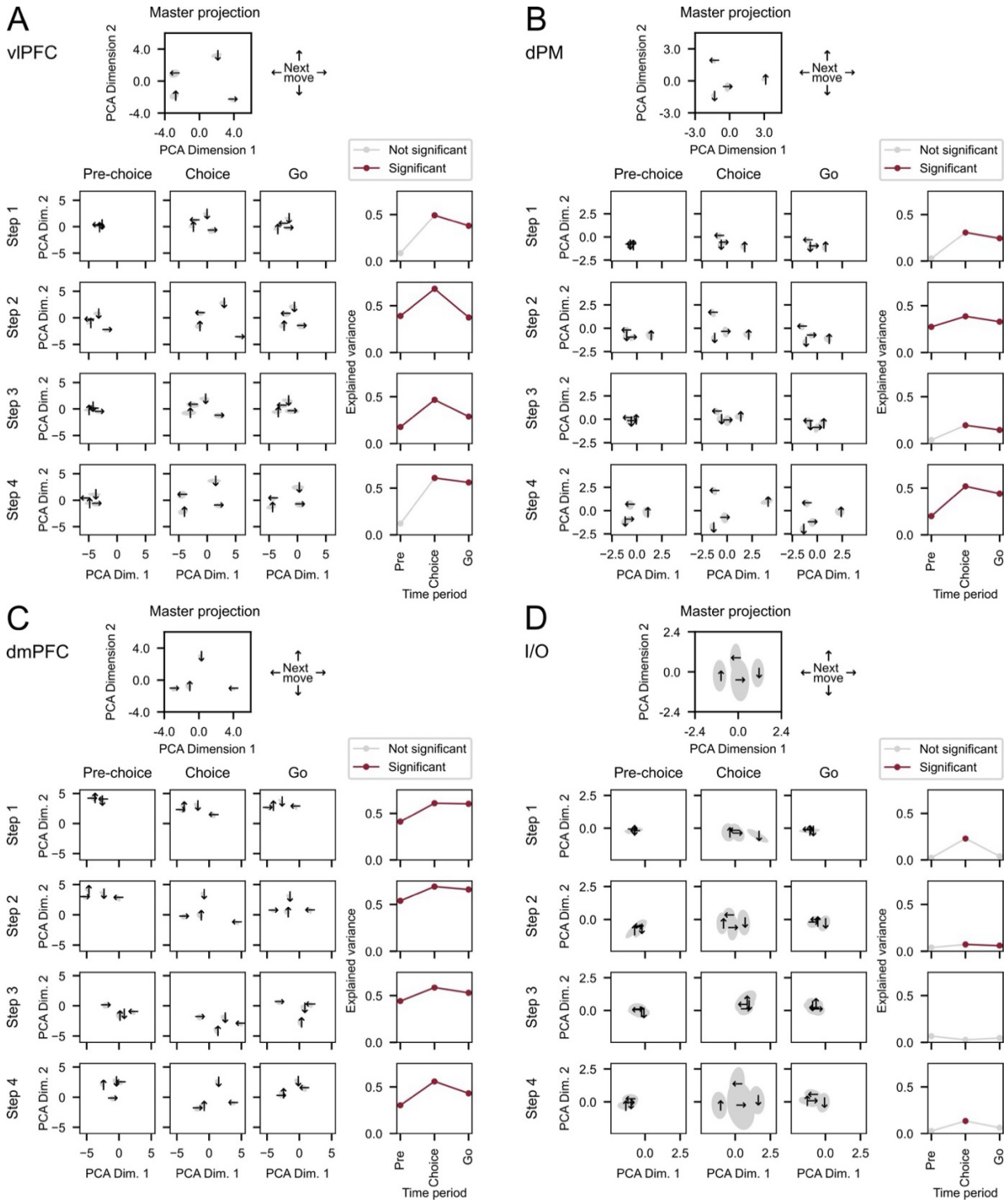

Fig. 5. **Move spaces**. A - vlPFC, B - dPM, C – dmPFC, D – I/O. For each region, the top panel shows projections into a master space derived from data averaged over four goal locations for

each move (choice periods from steps 2 (2-step problems only) and 4). Lower rows show projections into this master space for data from individual time windows in each step (left three panels), with proportion of explained variance in each window to the right (purple, $p < .05$, FDR corrected). In each row, data are sorted according to the move made on this step. Step 2 row takes data only from 2-step problems. Ellipses show confidence intervals derived by bootstrap resampling.

For a closer examination of neural dynamics, we focused on step 1, when onset of the choice stimulus strongly drove move selection, and the transition into step 2, when the selected move for step 1 was complete and the expected step 2 move was prepared. For this analysis we used 50 ms windows, covering the ranges -300 to +400 ms from choice 1 onset, -200 to +100 ms from choice 1 go signal, and -400 to +100 ms from choice 2 onset. For each window, we projected data into the move space, as defined above, and measured the distance of projected data from canonical positions for the four moves (fig. 5, top panel for each region). In fig. 6, we plot distance from the canonical position for the selected move 1, the prepared move 2, and for comparison, the two other moves (baseline, matching neither move 1 nor 2).

Resembling the above results for dmPFC, even prior to onset of the choice 1 stimulus, the data suggest weak bias towards both of the moves associated with the current goal (note that, for each goal, the step 2 move prepared following step 1 was also the alternative move that could itself have been cued for step 1; see fig. 1A). Though visible in vlPFC, dPM and dmPFC, these differences from baseline were small and mostly nonsignificant. Following onset of the choice stimulus, the representation shifted towards the selected move 1. This shift was seen first in vlPFC, followed by dPM and finally, more weakly, in dmPFC. Move 1 coding was sustained up to the time of the go signal, then followed by a rapid shift away from move 1 and towards the prepared move 2. In vlPFC, this shift towards move 2 was significant by 200-250 ms prior to

choice 2, only 150-200 ms after completing the move 1 saccade (fig. 1A, right), with a slightly slower timecourse in dPM, and again, appeared only later and more weakly in dmPFC.

In 4-step problems, with onset of the choice 2 stimulus, the prepared move towards the goal had to be abandoned and a new move selected. Though move coding became disorganized (fig. S2), by the time of the go signal, there were shifts away from the move initially prepared and towards the move selected.

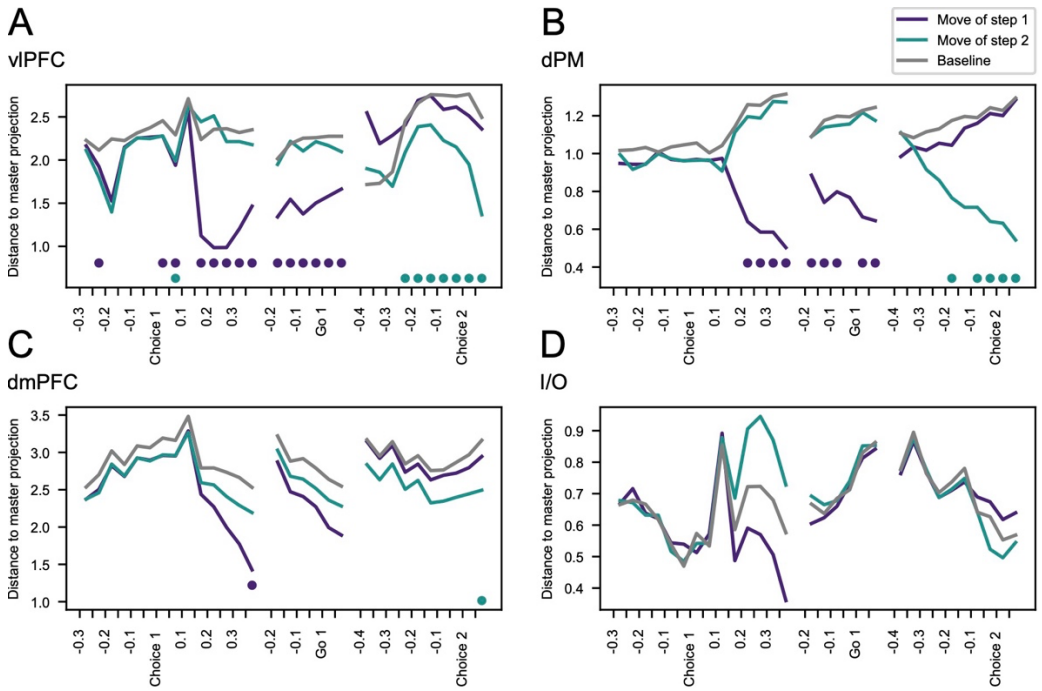

<u>Fig. 6.</u> Distances of projected data from canonical positions in master move space. Data are shown for 50 ms windows spanning choices 1 and 2. A - vlPFC, B - dPM, C – dmPFC, D – I/O. Purple – distance of projected data from master position for the required move 1. Aqua – distance from master position for the required move 2. Grey – mean distance from master position for remaining two moves (baseline). Bottom dots – difference from baseline significant at $p < .05$, FDR corrected.

Together, these results show that move coding in response to a visual input arose first in vlPFC, followed shortly afterwards by dPM. Move coding was strong also in dmPFC (fig. 4), but weak

in I/O. Across regions, once a move was completed, there was rapid transition to preparation for the next.

Orthogonality of spaces

To assess orthogonality of location and move spaces, we projected data for the four moves (window +200 to +400 ms) into the location space, and data for the four goals (window -200 to +100 ms) into the move space. In each case, the data projected were those used in the original definition of spaces, combining steps 2 and 4 to obtain a mean for each goal position, averaged over possible moves, and a mean for each move, averaged over possible goals. We asked what proportion of variance between the four moves was captured by projections in the location space, and vice versa. For vlPFC, dPM and I/O, spaces were close to orthogonal with <8% of variance captured in these cross-projections (<5% for all cases except I/O, projection of moves into location space). For dmPFC, however, there was some overlap between spaces (22% of variance for move projected into location space, 28% for the reverse).

Problem structure

Our final analyses concerned abstract problem structure separate from the specific content of any one problem. For an initial overview, we examined activity patterns for each successive period of a problem. For each of the periods previously defined (figs. 3, 5; three periods for each step), and for each of the four goals, we calculated mean normalized spike rate for each neuron. For this analysis we also added two windows in the initial goal presentation period, 100-400 and 400-900 ms following onset of the goal stimulus. Vectors of spike rate across all recorded neurons were then correlated across two independent halves of the data (see Materials and Methods). The result was a matrix of correlations between activity patterns for each trial period

x goal. This overview of the data suggested three potential patterns of interest (fig. S3). First, there was a strong diagonal, showing that patterns of activity changed substantially between each successive time window of problem solution. Second, there was a suggestion of hierarchical structure, with stronger correlations within than between successive steps, and between steps, stronger correlations for same versus different time windows. Importantly, these impressions remained even for correlations between problems with different goals, suggesting that they concerned abstract problem structure rather than specific problem content.

For formal analysis, we focused just on windows of steps 1 and 2 (2-step problems), for which there were most data. To focus on abstract problem structure, we considered only correlations between steps with different goals, current positions and moves. To this end we produced a 48 x 48 matrix, distinguishing 8 possible cases in step 1 (4 goals x 2 first moves), 8 possible cases in step 2 (4 goals x 2 current positions/next moves), and 3 windows within each step. For each of the 16 x 16 pairs of cases, there was a 3 x 3 matrix of correlations between time periods. We removed all pairs of cases that had the same goal, current position or move. Note that all correlations within step 1 were removed, since all step 1 problems had the same current position. Note also that now there was no need to separate the data into independent halves, since the major diagonal (correlation of each case with itself) was removed. Among the remaining pairs of cases (step 1 cases with step 2 cases, and correlations between different step 2 cases), we averaged the 3 x 3 correlation matrices. The result was a matrix of 3 (step 2 windows) x 6 (step 1 plus step 2 windows) mean correlations (fig. 7).

For all four regions, the impressions from the overall correlation matrix were confirmed. The strongest correlations were for same step, same window, confirming that, across the network, patterns of neural activity carry an abstract code of progress through the problem. Next

strongest, except in vlPFC, were correlations for same step, different window, indicating a code of current step, followed by different step, same window, indicating a code of progress through the current step. For all regions, correlations of all these cases were stronger than for a baseline of different step, different window ($p < .001$ for all comparisons).

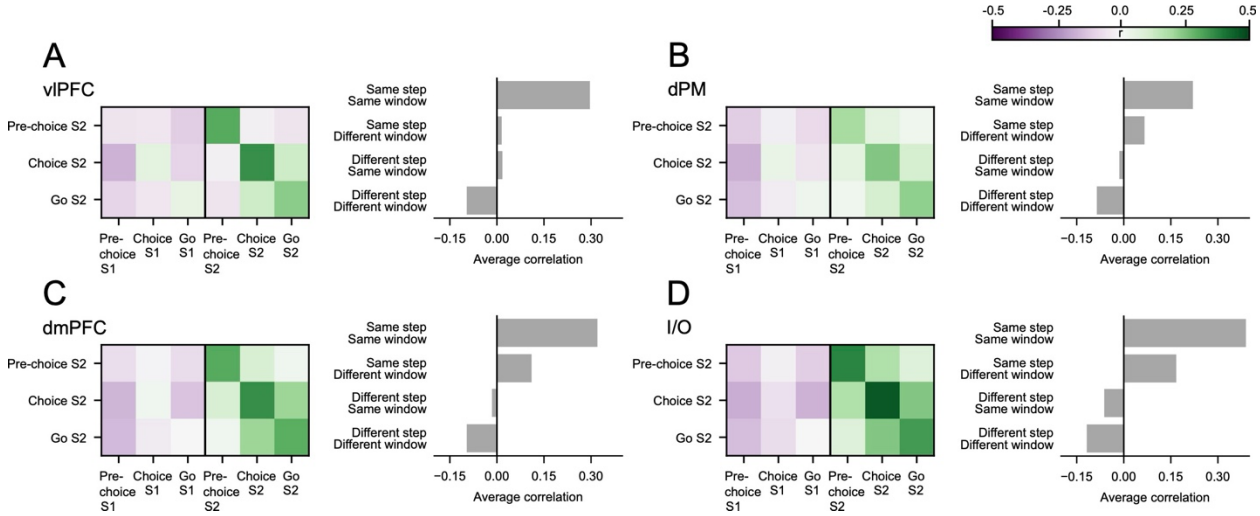

Fig. 7. Correlation of cross-neuron activity patterns. A - vlPFC, B - dPM, C – dmPFC, D – I/O. For each region, left part shows mean correlations of each step 2 (S2) window with step 1 (S1) and step 2 (S2) windows. Data are means across all step 1 - step 2 and step 2 - step 2 pairs that have different goals, current positions and moves. Note that step 2 – step 2 matrix is symmetrical (see Materials and Methods). Right shows mean correlations for same step same window, same step different window, different step same window, and different step different window.

Stronger correlations for same step, different window than for different step, different window might in part reflect simple temporal separation. To assess this, we compared correlations for step 2, pre-choice with step 1, go and step 2, go. Temporal separation for these cases was approximately matched (for monkey A, mean time between step 1 go and step 2 pre-choice 772 ms; mean time between step 2 pre-choice and step 2 go 900 ms; for animal 2, respectively 624 and 700 ms), but still, the correlation for step 2, pre-choice with step 2 go was significantly

greater than the correlation for step 2, pre-choice with step 1, go ($p < .02$, .001, .005 and .001 respectively for vlPFC, dPM, dmPFC, I/O).

Discussion

Complex, goal-directed cognition calls for representation of current state, goal state, and actions chosen to diminish the distance between the two, often organized into a hierarchical structure of goals and subgoals. As monkeys plan a route through a maze, our data show all these properties in an extended frontal lobe network, putatively based on the extended MD network of human cognition. In line with human imaging, our results show strongly overlapping properties in four frontal lobe regions, but at the same time, clear quantitative differences and partial specialisations.

In vlPFC, we saw the strongest immediate coding of sensory input, including a cue to the current target location, choice alternatives indicating the required first move, and an indication of current route type (2- or 4-step). Orthogonal representational spaces in vlPFC coded current location and move, and compared with move spaces in other regions, vlPFC showed the most rapid change as a move was chosen. Previous findings have suggested vlPFC as an attentional hub (*28*), with strong coding of both spatial and nonspatial features of a current task (*29-30*), and widespread cortical connectivity (*31*). Our data suggest a central role in the individual operations of each task stage – encoding a target, responding to sensory input and selecting an individual move.

In dmPFC, uniquely, there was a sustained signal of the final goal, beginning when this goal was first cued and lasting until problem end. Much previous research links dmPFC to reward processing (e.g. *10*, *20, 32*), based on extensive connectivity to reward systems (*33*). dmPFC has

frequently been linked with energizing behavior (*34*) and a willingness to meet challenges (*35-36*). An influential proposal links dmPFC to the tradeoff between prospective rewards and the effort needed to obtain them (*37*). A plausible possibility is that a sustained goal code in the maze task is linked to the reward obtained on reaching it. This sustained goal signal, we suggest, energises a series of steps or sub-goals along the path to its achievement. Though a number of prior proposals have concerned the separate functions of dorsomedial and lateral frontal cortex (e.g. *38-39*), by separating goal coding from coding of individual task steps, we were able to show that one strong property of dmPFC is the stability of coding a higher-level goal.

In dPM, as in vlPFC, there was rapid move coding following onset of a choice stimulus, as expected for a motor region linked to primary motor cortex, and involved in both manual and saccadic movements (*40*). In I/O, there was weak coding of sensory input, locations and moves. Instead, there was strong response to input that distinguished short and long routes to the goal. Insula coding of progress towards a goal has been shown previously (*15*, *19*). Plausibly, this signal may be related to the strong autonomic connectivity of the insula (*41*), and anticipatory arousal linked to goal proximity.

Across regions, despite these partial specialisations, our data also showed substantial overlap of coding properties. In dPM and I/O, for example, there was coding of both current position in the maze, resembling vlPFC, and goal position, resembling dmPFC. Though motor signals emerged most rapidly in vlPFC and dPM, there was also a clear move space in dmPFC, and to some extent also in I/O. When moves were partially or whole predictable, anticipatory move signals were seen across vlPFC, dPM and dmPFC. Though vlPFC responded most rapidly to new sensory input, these rapid responses were followed by more slowly-developing activity across all regions, and for inputs indicating goal, move or route length. Strong interconnectivity between

frontal regions (*5-6*) provides a basis for substantial information sharing. Our data suggest that, in each region, there are often copies of information more strongly coded elsewhere. In each region, to a large extent, different aspects of the monkey's problem were encoded in orthogonal state spaces, suggesting a medium for minimized interference between these distinct codes.

One strong common element across all four recording regions was a strong, hierarchical representation of abstract problem structure. In each region, activity patterns were strongly correlated for the same time window in the same task step, even when goals, current positions and moves all differed. Patterns were more similar within than between task steps, suggesting a coarse, step-wise code of task structure, and between steps, patterns were more similar for the same than for different time windows, suggesting an abstract code of progress within each step. Strong coding of the current point in progress from problem start to goal matches previous findings in both monkeys (*42*) and mice (*43*). Our data suggest that coding of abstract problem structure is a broad principle of prefrontal activity, perhaps providing a general scaffold onto which an individual problem solution can be attached (*44*).

Our results leave many questions open. Strong overlap in the response properties of different regions suggests the likelihood of communication, with each region influencing activity in the others. For example, the finding of early sensory responses in vlPFC might suggest that sensory information is distributed from this region to others. Current data, however, cannot test such hypotheses. Our selection of regions as potential matches to human MD regions is tentative, especially for I/O where we have little direct evidence of correspondence. Though our data suggest partial specialisations between frontal regions – for example, strong coding of sensory input and current state in vlPFC, and stable goal coding in dmPFC – these specialisations call for examination in a wider range of multi-step tasks, including pursuit of nonspatial goals.

Meanwhile, our data suggest how the distributed components of a frontal lobe network encode the essential features – goal, current state, component moves, and hierarchical problem structure - in complex, temporally extended, goal-directed behavior. They suggest a network with partial specialisations arising from distinct connectivity, but broad co-recruitment reflecting information exchange. Evolving activity across this network builds the control program for extended, goal-directed behavior.

Materials and methods

Subjects

Subjects were two male rhesus monkeys (Macaca mulatta), each weighing 12 kg. Experiments were performed in accordance with the Animals (Scientific Procedures) Act 1986 of the UK; all procedures were licensed by a Home Office Project License obtained after review by Oxford University's Animal Care and Ethical Review committee, and were in compliance with the guidelines of the European Community for the care and use of laboratory animals (EUVD, European Union directive 86/609/EEC).

Task

In each session, the monkeys solved a series of problems defined in a 5 x 5 square maze, presented as a grid of lines on a computer screen (fig. 1A). Lines were white on a grey background. The 5 x 5 maze locations were defined by intersections between the lines of the grid. At each step of the solution, the current location was defined by the animal's fixation on one of these intersections.

Moves consisted of a single step, i.e. a saccade from the current location to an immediately adjacent location. From a starting point in the central location, the task was to reach a specified goal location in a series of single steps. The goal was always located at one of the four corners of the inner 3 x 3 square of locations (fig. 1A, left). A correct trial consisted of taking the shortest route to the goal, considering the paths available at each choice. The types of trial were randomized between short (easy) consisting of only 2 saccades (2-step) before reaching the final goal, and long (difficult) with 4 saccades (4-step) (fig. 1A, left).

Timings are illustrated in fig. 1A (right). At the start of each problem, a dark green fixation point appeared at grid center. Fixation on this point was required within 3 s. Once fixation was initiated, the dark green turned into bright green and after 100 ms a white diamond (cursor) joined the fixation point. After 200 ms a blue circle (target) appeared at the final goal location of the current trial and remained on the screen for 900 ms while the monkeys kept fixating in the center. Following the disappearance of this goal stimulus, there was a 300 ms delay, and then the four choice options of the first step were presented. Two dark green dots and two red dots appeared simultaneously at the four locations immediately adjacent to the central one (where the monkeys were still fixating). Red dots indicated steps unavailable for selection on this trial. Green dots indicated available choices, one of which was correct as it indicated a move towards the final goal. Following a delay period (randomly 300, 900, or 1500 ms for monkey A; 500 or 900 ms for monkey B), a go signal was presented. For monkey A, this go signal was simply the disappearance of the green fixation point; for monkey B this was accompanied by a small drop of reward (fruit smoothie). Following this go signal, the monkey had 500 ms (monkey A) or 350 ms (monkey B) to initiate a saccade to the correct choice location and 30 ms (monkey A) or 20 ms (monkey B) to complete it. Once the saccade was complete, if the choice was correct, the

new fixation point changed to bright green and all the other old stimuli (center fixation point, white cursor, other choices) disappeared. While the monkey held fixation, the second step of the trial began. With the same timing as for the first step, the cursor appeared after 100 ms and the second set of 4 choices appeared after a further 300 ms, presented for the same variable delay as before and followed by the go signal and saccade. In 2-step trials, one of the choice 2 options lay at the final goal location, allowing the trial to be completed (fig. 1A, left, orange lines). In this case, after the correct saccade was made, the blue final target reappeared and a smoothie reward was delivered. On 4-step trials, however, monkeys needed to take a detour to the outer ring of the grid (fig. 1A, left, green lines). In this case, at step 2, the final target location was colored red, along with the previous fixation point at maze center. From the remaining two green choices, the monkey was required to choose the step to the outer ring. The third and fourth steps then followed the same structure as steps 1 and 2, though in each case, to enforce the correct route (fig. 1A, left), there was only one red dot (in the location just left) and two green. At the end of step 4, when one of the green choices lay at the final goal location, the trial ended as before with reappearance of the blue target and reward delivery.

On completion of each trial, all stimuli except the grid disappeared and there was an intertrial interval of 1800 ms. Throughout the problem, any error (wrong choice; fixation break; late response) led to problem termination, with a red error cue at screen center and no reward.

Task events were controlled by REX real-time data acquisition and laboratory control software (developed by the National Institutes of Health), with displays presented on a 44 cm LED screen placed 30 cm in front of the monkey's eyes. The 5 x 5 maze measured 32 x 32 deg visual angle. Fixation point and red/green choice cues each measured 1.5 x 1.5 deg, while blue targets measured 3 x 3 deg. Eye position was sampled at 120 Hz using an infrared tracking system

(ASL EYE-TRAC; Applied Science Laboratories www.asleyetracking.com), with each correct fixation required within a window of 3 x 3 deg. The eye tracker was re-calibrated at the start of each session.

Surgery and recordings

For each animal, in two surgeries, a titanium head holder and recording chamber (Gray Matter Research) were sterotaxically implanted on the skull. Chambers were custom designed from a MRI based skull model of each monkey and placed over the lateral prefrontal cortex of the left hemisphere, giving access to dorsomedial and lateral frontal surfaces, along with anterior insula and surrounding orbitofrontal cortex. In a third procedure, a craniotomy was performed under each chamber to mount a 128-channel semichronic microdrive (LS-128-FL, Gray Matter Research). All surgical procedures were aseptic and carried out under general anaesthesia. At the end of the experiments, animals were deeply anesthetized with barbiturate and then perfused through the heart with heparinized saline followed by 10% formaldehyde in saline. The brains were removed for histology and recording locations confirmed.

Within the microdrive, each of the 128 single-contact tungsten electrodes was independently and manually movable in depth. Spacing between electrodes was 1.5 mm. The microdrive was interfaced with a multichannel data acquisition system (Cerebus System, Blackrock Microsystems). Raw extracellular signals were amplified, filtered (250 Hz to 5 kHz), and recorded in reference to the titanium head holder. Single action potentials were extracted and saved together with behavioral event codes in a file used for offline sorting and analysis.

Initial spike sorting was performed online through the Blackrock interface before the start of each recording session. Sorting was then adjusted while the monkeys were performing the task

and finalised offline (Plexon Offline sorting, version 4.7.1). In most cases, to ensure recording of new neurons, electrodes were advanced at least 62.5µ before every session. If this was not done, a Matlab-based algorithm was used to remove cases of repeat recording from the same neuron (https://uk.mathworks.com/matlabcentral/fileexchange/30113-tracking-neurons-over-multiple-days).

Data analysis

Analysis scripts were written in Matlab (MathWorks) and Python.

To assess sensory information coding (fig. 2), for each cell, firing rates were examined by ANOVA with factors goal (goal presentation period), goal x horizontal/vertical choice available (choice 1 period) and goal x 2- vs 4-step (choice 2 period). From each ANOVA we calculated proportion of explained variance (PEV) for the factor of interest, and averaged this across all cells in each region. PEV was measured by the partial ω^2 index of effect size, calculated by the formula

$$\omega^2 = df_{effect} \times (MS_{effect} - MSE) / (SS_{effect} + (N_{total} - df_{effect}) \times MSE)$$

where df_{effect} is degrees of freedom for the factor of interest (target, choice, problem type), MS_{effect} is the mean square for the factor, SS_{effect} is the sum of squares for the factor, MSE is the mean square error, and N_{total} is the total number of observations (problems). Within each region, randomization tests were used to assess the significance of mean PEV values. For each neuron, labels for the factor of interest were randomized across problems, followed by re-calculation of mean PEV across cells. The PEV value for the true data was compared with the distribution obtained from 1000 repetitions of this randomization, and the *p* value determined by the

proportion of randomized values greater than or equal to the true value. This procedure was repeated for each time window, and for each region, the criterion for significance was set at $p < .05$ corrected for multiple comparisons (time windows) by false discovery rate (FDR; *45*). A similar procedure was used to compare PEV between regions, this time randomising just the region labels of each neuron.

To construct location and move spaces (figs. 3, 5), we used principal components analysis (PCA). For each neuron, missing data for a combination of location x move were filled in with the mean of other values. 95% confidence intervals (figs. 3, 5, ellipses) were constructed by bootstrap resampling of problems for each neuron. For each analysis window, we created 1000 bootstrapped projections, aligned by Procrustes transformation to the original projections.

To assess how much variance each space explained in successive problem periods (figs. 3, 5, rightmost panel in each row), we used a fully cross-validated approach. Two parallel data sets were created by randomly separating problems for each neuron into two groups, and PCA spaces were created for each half of the data. Data for each half were then projected onto the first two components of the PCA from the other half, and then reverse projected into the original data space. We then calculated the variance in the original data explained by the reconstructed data. Figures show the mean result from the two directions of cross-validation. To test significance, we repeated this process 1000 times while shuffling condition labels. The *p* value was given by the proportion of randomized values greater than or equal to the true value, FDR corrected for all comparisons for a given region.

To correlate activity patterns across problem periods, problems for each neuron were split into two equally-sized sets. All firing rates for a given neuron were normalized (division by mean

firing rate across the period from goal onset to end of step 2). Activity patterns for each region, and each half of the data, were then constructed as vectors of normalized firing rate across all neurons. Where a value for a given goal x time window was missing, it was filled in with the mean of that same time window for other goals. Similarity between vectors (fig. 7) was measured by Pearson's *r*. Correlations were averaged (fig. 7, histograms) by *r* to *z* transformation.

For analyses in figs. 4, 6 and 7, significance values were obtained by bootstrap resampling. For each of 1000 repetitions, we drew samples of cells from each region, matched in size to the original data but sampled with replacement. The *p* value was given by the proportion of samples with a mean difference between regions opposite to the majority, multiplied by 2 for a two-tailed test. The criterion for significance was set at $p < .05$, FDR corrected across time-points for each comparison in fig. 6.

Acknowledgments

Funding: This work was supported by Medical Research Council UK Program MC_UU_00030/7 and Wellcome Trust Grant 101092/Z/13/Z. Author contributions: V. M. – conceptualization, data collection, data analysis, manuscript review; J. A. – conceptualization, data analysis, manuscript review; M. K. – planning and implementation of recording methods, manuscript review; M. J. B. – supervision, funding, manuscript review; J. D. – conceptualization, supervision, funding, data analysis, original draft of manuscript.

References

1. R. E. Passingham, S. P. Wise, *The neurobiology of the prefrontal cortex: Anatomy, evolution, and the origin of insight*. (Oxford University Press, Oxford, 2012).

2. S. C. Rao, G. Rainer, E. K. Miller, Integration of what and where in the primate prefrontal cortex. *Science* **276**, 821-824 (1997).

3. H. Tang, R. Bartolo, B. B. Averbeck, Reward-related choices determine information timing and flow across macaque lateral prefrontal cortex. *Nat Commun* **12**, 894 (2021).

4. L. T. Hunt *et al.*, Triple dissociation of attention and decision computations across prefrontal cortex. *Nat. Neurosci.* **21**, 1471-1481 (2018).

5. B. B. Averbeck, M. Seo, The statistical neuroanatomy of frontal networks in the macaque. *PLoS Computational Biology* **4**, e1000050 (2008).

6. M. L. Pucak, J. B. Levitt, J. S. Lund, D. A. Lewis, Patterns of intrinsic and associational circuitry in monkey prefrontal cortex. *J. Comp. Neurol.* **376**, 614-630 (1996).

7. J. Duncan, The multiple-demand (MD) system of the primate brain: Mental programs for intelligent behaviour. *Trends in Cognitive Sciences* **14**, 172-179 (2010).

8. J. Duncan, M. Assem, S. Shashidhara, Integrated intelligence from distributed brain activity. . *Trends in Cognitive Sciences* **24**, 838-852 (2020).

9. M. Assem, M. F. Glasser, D. C. Van Essen, J. Duncan, A domain-general cognitive core defined in multimodally parcellated human cortex. *Cereb. Cortex* **30**, 4361-4380 (2020).

10. K. Amemori, S. Amemori, A. M. Graybiel, Motivation and affective judgments differentially recruit neurons in the primate dorsolateral prefrontal and anterior cingulate cortex. *J. Neurosci.* **35**, 1939-1953 (2015).

11. R. Baez-Mendoza, E. P. Mastrobattista, A. J. Wang, Z. M. Williams, Social agent identity cells in the prefrontal cortex of interacting groups of primates. *Science* **374**, eabb4149 (2021).

12. S. E. Cavanagh, J. P. Towers, J. D. Wallis, L. T. Hunt, S. W. Kennerley, Reconciling persistent and dynamic hypotheses of working memory coding in prefrontal cortex. *Nat Commun* **9**, 3498 (2018).

13. K. Johnston, H. M. Levin, M. J. Koval, S. Everling, Top-down control-signal dynamics in anterior cingulate and prefrontal cortex neurons following task switching. *Neuron* **53**, 453-462 (2007).

14. R. F. Loonis, S. L. Brincat, E. G. Antzoulatos, E. K. Miller, A Meta-Analysis Suggests Different Neural Correlates for Implicit and Explicit Learning. *Neuron* **96**, 521-534 e527 (2017).

15. T. Mizuhiki, B. J. Richmond, M. Shidara, Mode changes in activity of single neurons in anterior insular cortex across trials during multi-trial reward schedules. *Neurosci. Res.* **57**, 587-591 (2007).

16. H. Mushiake, N. Saito, K. Sakamoto, Y. Itoyama, J. Tanji, Activity in the lateral prefrontal cortex reflects multiple steps of future events in action plans. *Neuron* **50**, 631-641 (2006).

17. T. Nakajima, R. Hosaka, H. Mushiake, Complementary Roles of Primate Dorsal Premotor and Pre-Supplementary Motor Areas to the Control of Motor Sequences. *J. Neurosci.* **42**, 6946-6965 (2022).

18. D. Vallentin, S. Bongard, A. Nieder, Numerical rule coding in the prefrontal, premotor, and posterior parietal cortices of macaques. *J. Neurosci.* **32**, 6621-6630 (2012).

19. Y. P. Yang, X. Li, V. Stuphorn, Primate anterior insular cortex represents economic decision variables proposed by prospect theory. *Nat Commun* **13**, 717 (2022).

20. S. B. M. Yoo, J. C. Tu, S. T. Piantadosi, B. Y. Hayden, The neural basis of predictive pursuit. *Nat. Neurosci.* **23**, 252-259 (2020).

21. M. Rothe, R. Quilodran, J. Sallet, E. Procyk, Coordination of high gamma activity in anterior cingulate and lateral prefrontal cortical areas during adaptation. *J. Neurosci.* **31**, 11110-11117 (2011).

22. D. Y. Kimberg, M. J. Farah, A unified account of cognitive impairments following frontal lobe damage: The role of working memory in complex, organized behavior. *J. Exp. Psychol. Gen.* **122**, 411-428 (1993).

23. J. Duncan, Construction and use of mental models: Organizing principles for the science of brain and mind. *Neuropsychologia* **207**, 109062 (2025).

24. G. A. Miller, E. Galanter, K. H. Pribram, *Plans and the structure of behavior*. (Holt Rinehart and Winston., New York NY, 1960).

25. A. Newell, J. C. Shaw, H. A. Simon, Elements of a theory of human problem solving. *Psychol. Rev.* **65**, 151-166 (1958).

26. C. Amiez *et al.*, A revised perspective on the evolution of the lateral frontal cortex in primates. *Sci Adv* **9**, eadf9445 (2023).

27. K. S. Saleem, N. K. Logothetis, *A combined MRI and histology atlas of the rhesus monkey brain in stereotaxic coordinates (2nd edition)*. (Academic Press, London, 2012).

28. L. R. Trambaiolli *et al.*, Anatomical and functional connectivity support the existence of a salience network node within the caudal ventrolateral prefrontal cortex. *Elife* **11**, (2022).

29. S. W. Kennerley, J. D. Wallis, Reward-dependent modulation of working memory in lateral prefrontal cortex. *J. Neurosci.* **29**, 3259-3270 (2009).

30. M. Kadohisa *et al.*, Frontal and temporal coding dynamics in successive steps of complex behavior. *Neuron* **111**, 430-443 e433 (2023).

31. F. X. Neubert, R. B. Mars, A. G. Thomas, J. Sallet, M. F. Rushworth, Comparison of human ventral frontal cortex areas for cognitive control and language with areas in monkey frontal cortex. *Neuron* **81**, 700-713 (2014).

32. S. W. Kennerley, A. F. Dahmubed, A. H. Lara, J. D. Wallis, Neurons in the frontal lobe encode the value of multiple decision variables. *Jpurnal of Cognitive Neuroscience* **21**, 1162-1178 (2009).

33. S. R. Heilbronner, B. Y. Hayden, Dorsal Anterior Cingulate Cortex: A Bottom-Up View. *Annu. Rev. Neurosci.* **39**, 149-170 (2016).

34. T. Shallice, D. T. Stuss, M. P. Alexander, T. W. Picton, D. Derkzen, The multiple dimensions of sustained attention. *Cortex* **44**, 794-805 (2008).

35. J. Parvizi, V. Rangarajan, W. R. Shirer, N. Desai, M. D. Greicius, The will to persevere induced by electrical stimulation of the human cingulate gyrus. *Neuron* **80**, 1359-1367 (2013).

36. M. E. Walton, D. M. Bannerman, M. F. Rushworth, The role of rat medial frontal cortex in effort-based decision making. *J. Neurosci.* **22**, 10996-11003 (2002).

37. A. Shenhav, M. M. Botvinick, J. D. Cohen, The expected value of control: An integrative theory of anterior cingulate cortex function. *Neuron* **79**, 217-240 (2013).

38. M. M. Botvinick, T. S. Braver, D. M. Barch, S. C. Carter, J. D. Cohen, Conflict monitoring and cognitive control. *Psychol. Rev.* **108**, 624-652 (2001).

39. N. U. Dosenbach *et al.*, Distinct brain networks for adaptive and stable task control in humans. *Proc. Natl. Acad. Sci. U. S. A.* **104**, 11073-11078 (2007).

40. B. Pesaran, M. J. Nelson, R. A. Andersen, A relative position code for saccades in dorsal premotor cortex. *J. Neurosci.* **30**, 6527-6537 (2010).

41. D. Roquet, F. Conti, Disentangling the Association between the Insula and the Autonomic Nervous System. *J. Neurosci.* **41**, 3051-3053 (2021).

42. N. Sigala, M. Kusunoki, I. Nimmo-Smith, D. Gaffan, J. Duncan, Hierarchical coding for sequential task events in the monkey prefrontal cortex. *Proc. Natl. Acad. Sci. U. S. A.* **105**, 11969-11974 (2008).

43. M. El-Gaby *et al.*, A cellular basis for mapping behavioural structure. *bioRxiv*, (2023).

44. J. X. Wang *et al.*, Prefrontal cortex as a meta-reinforcement learning system. *Nat. Neurosci.* **21**, 860-868 (2018).

45. Y. Benjamini, Y. Hochberg, Controlling the false discovery rate: A practical and powerful approach to multiple testing. *Journal of the Royal Statistical Society. Series B.* **57**, 289-300 (1995).

Supplementary figures

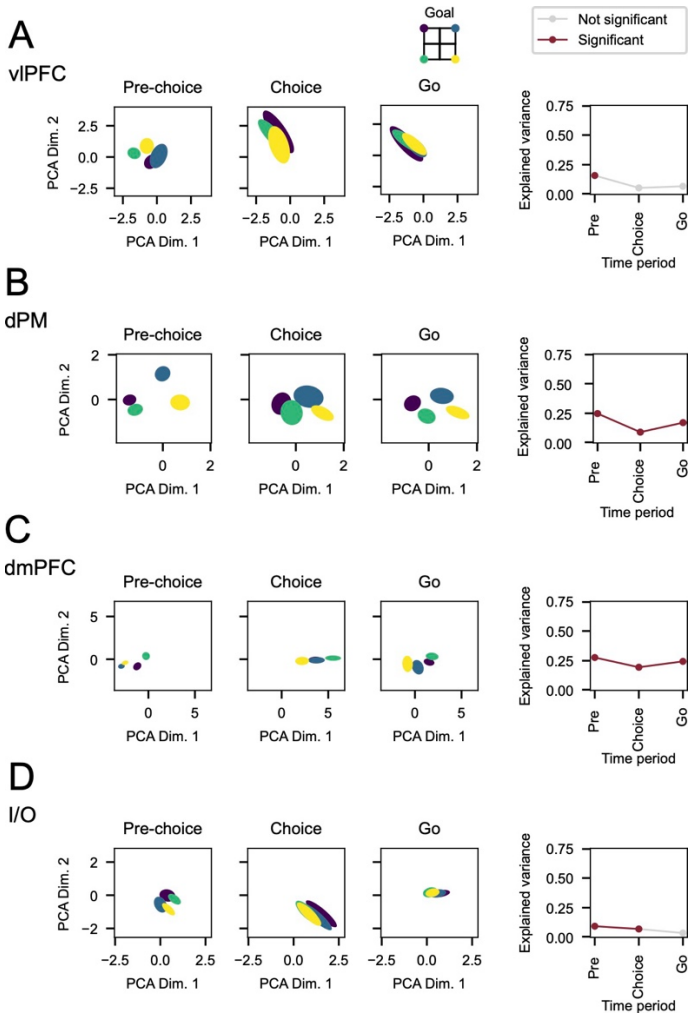

Fig. S1. Projections of data from step 2, 4-step problems into location spaces. A - vlPFC, B - dPM, C – dmPFC, D – I/O. Conventions as fig. 3.

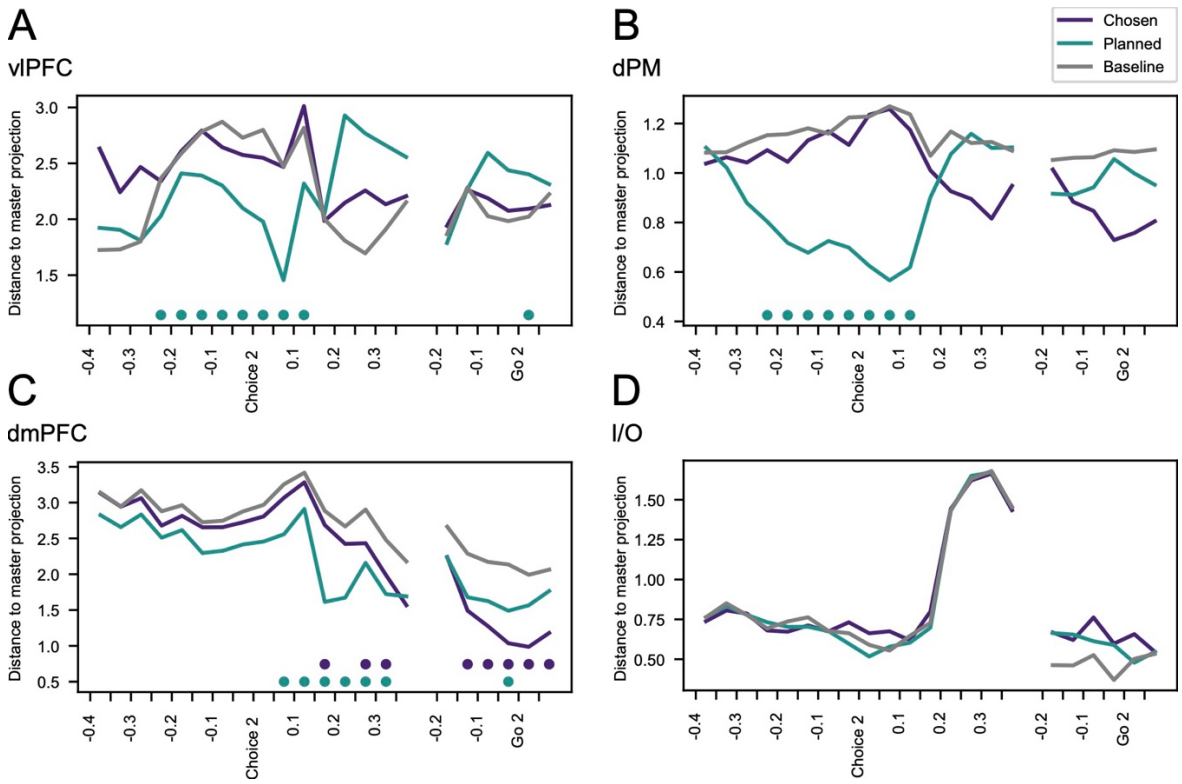

<u>Fig. S2</u>. 4-step problems: Distances of projected data from canonical positions in master move space. Data are shown for 50 ms windows spanning choice 2. A - vlPFC, B - dPM, C – dmPFC, D – I/O. Purple – distance of projected data from master position for the required 4-step move. Aqua – distance from master position for the planned 2-step move. Grey – mean distance from master position for remaining two moves (baseline). Bottom dots – difference from baseline significant at $p < .05$, FDR corrected.

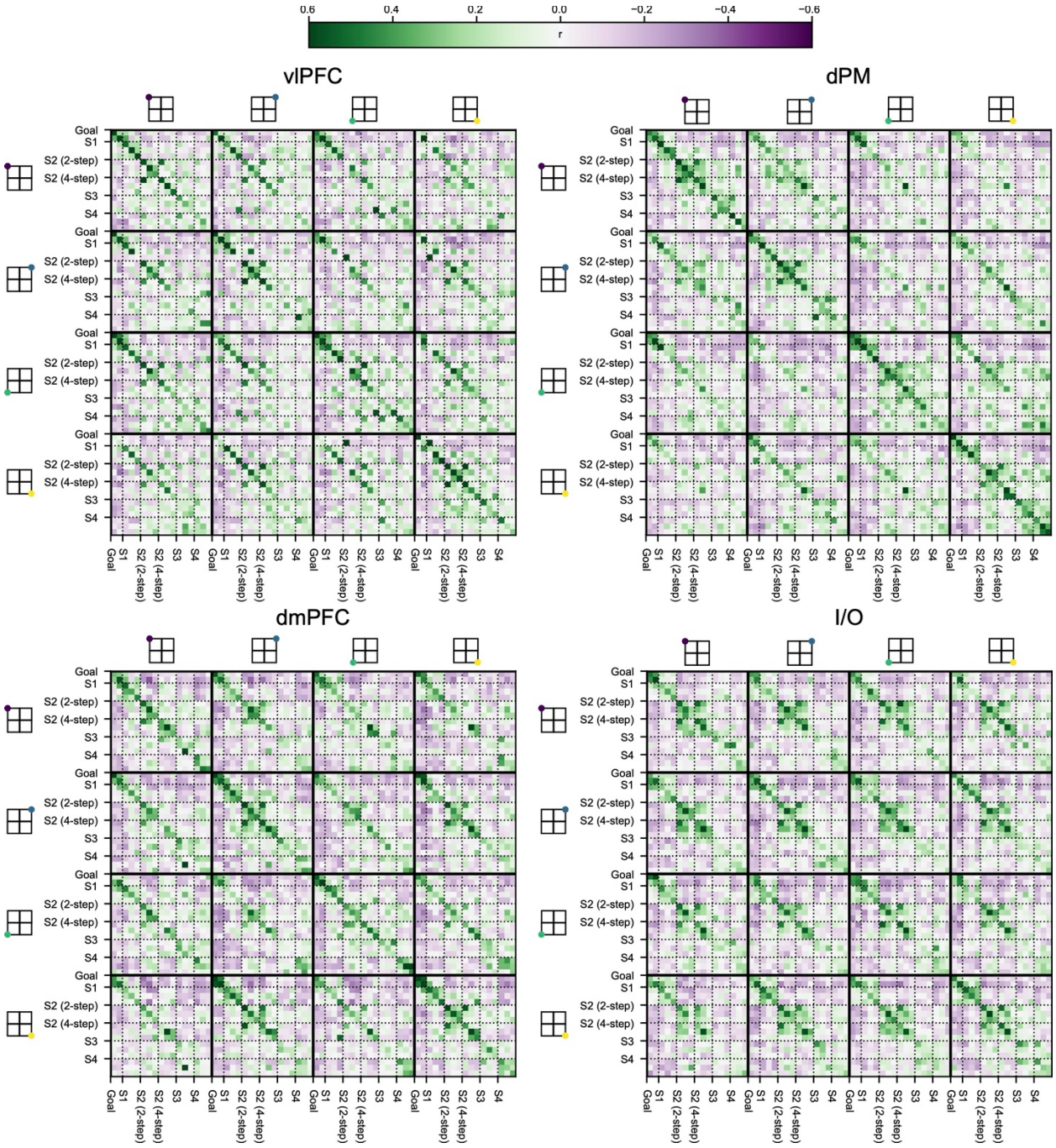

<u>Fig. S3</u>. Correlation of cross-neuron activity patterns. A - vlPFC, B - dPM, C – dmPFC, D – I/O. From top to bottom, 17 time windows for each goal include 2 for goal presentation (100-400 and 400-900 ms post onset), and 3 each (pre-choice, choice, go) for step 1, step 2 2-step, step 2 4-step, step 3, step 4 (S = step).